Electronic Supplementary Information

for

Transformation of benzocorrole isomer into pyrrole-containing polycyclic molecules via copper-mediated cleavage and annulation

Biju Basumatary,[#,a] Sawako Yada,[#,a] Shunsuke Oka,[b] Shigeki Mori,[c] Tatsuya Mori,[d] Tatsuki Abe, [a] Daisuke Kawaguchi, [a] Takuma Yasuda,*[d] Hiroyuki Furuta*[a] and Masatoshi Ishida*[b]

[a] Department of Applied Chemistry, Graduate School of Engineering, Kyushu University, Fukuoka 819-0395 (Japan), E-mail: furuta.hiroyuki.165@m.kyushu-u.ac.jp

[b] Department of Chemistry, Graduate School of Sciences, Tokyo Metropolitan University, Tokyo 192-0397 (Japan), E-mail: ishidam@tmu.ac.jp.

[c] Advanced Research Support Center, Ehime University, Matsuyama 790-8577 (Japan)

[d] Institute for Advanced Study, Kyushu University, Fukuoka 819-0395 (Japan), E-mail: yasuda@ifrc.kyushu-u.ac.jp

Table of Contents

1. Experimental Procedures

Materials and Instruments. Commercially available solvents and reagents were used without further purification unless otherwise mentioned. Thin-layer chromatography (TLC) was carried out on aluminium sheets coated with silica gel 60 F_{254} (Merck 5554). The precursor compound **3** was prepared according to the reported protocol.[s1] ^{1}H- and ^{19}F-NMR spectra were recorded on a JEOL ECX500 NMR spectrometer at ambient temperature (298 K), and chemical shifts are reported in ppm relative to the residual peaks of $CDCl_3$ (δ = 7.26 ppm), and CD_2Cl_2 (δ = 5.32 ppm) and trifluoroacetic acid as an external reference for ^{19}F (δ = −76.55 ppm). UV/vis/NIR spectra were measured on a JASCO V770 spectrophotometer. High-resolution mass (HRMS) spectra were obtained in fast atom bombardment (FAB mode) with 3-nitrobenzyl alcohol (NBA) as a matrix on a JEOL LMS-HX110 spectrometer. Cyclic voltammetry (CV) was carried out on a CH Instrument Model 620B (ALS) with an electrochemical system utilizing the three-electrode configuration consisting of glassy carbon (working electrode), platinum wire (counter electrode), and Ag/AgCl (reference electrode) in CH_2Cl_2 with 0.1 M *n*-tetrabutylammonium hexafluorophosphate ($TBAPF_6$) as a supporting electrolyte under argon. Potentials were calibrated with the ferrocenium/ferrocene (Fc^+/Fc) couple.

X-ray Crystallography. Single crystal X-ray structural analysis for **1** and **2** was performed on a Saturn equipped with a CCD detector (RIGAKU) using MoKα (graphite, monochromated, λ = 0.71069 Å) radiation. The data were corrected for Lorentz, polarization, and absorption effects. The structure was solved by the direct method of SIR2004 or SIR2011, or SHELXT Version 2014/5 and refined using the SHELXL-2013 or SHELXL-2014/7 program.[s2] All the positional parameters and thermal parameters of non-hydrogen atoms were refined anisotropically on F^2 by the full-matrix least-squares method. Hydrogen atoms were placed at the calculated positions and refined riding on their corresponding carbon atoms.

Femtosecond TA spectroscopy

Transient absorption spectra were determined by using a spectrometer system (Helios, Ultrafast Systems, FL, USA) with a regenerative amplified Ti:sapphire laser (Solstice, Spectra-Physics, CA, USA). The laser provided fundamental pulses with λ = 800 nm and a width of 100 fs (fwhm) at a repetition rate of 1 kHz, which were split into two beams with a beam splitter to generate pump and probe pulses. One of them was converted into pump pulses, which were mechanically modulated with a repetition rate of 500 Hz, with λ = 400 nm with a second harmonic generator. Another was converted into probe pulses with the λ regions from 450 to 750 nm (visible (VIS)). The cell cuvette was set in a holder and excited by pump pulses with a laser power of 200 μW.

OFET device fabrication and measurements.

OFET devices were fabricated in a top-contact, bottom-gate configuration on heavily doped n-type Si wafers with a thermally grown 300-nm-thick SiO_2 layer. The SiO_2/Si substrates were pretreated with a piranha solution at 90 °C for 1 h, and then copiously cleaned by sonication in deionized water, acetone, and isopropanol for 15 min and subjected to UV/ozone treatment for 30 min. The surface of the SiO_2/Si substrates was treated with octyltrichlorosilane (OTS) in dry toluene at 60 °C for 10 min to form a hydrophobic self-assembled monolayer. Single crystals were grown by drop-casting the solution on the OTS-treated SiO_2/Si substrates. Single-crystal OFET devices were completed by evaporating Au (thickness = 50 nm) through a shadow mask to define the source and drain electrodes with a channel length of 58–77 μm on top of each active layer. The transfer and output characteristics of the OFETs were measured using a B1500A semiconductor parameter analyzer (Keysight Technologies) in air at room temperature. Field-effect mobility (μ) was calculated in the saturation regime using the following equation: $I_D = (W/2L)\mu C_i(V_G – V_{th})^2$, where I_D is the drain current, W and L are the channel width and length, respectively, C_i is the capacitance per unit area of the gate dielectric (11.1 nF cm^{-2} for SiO_2/Si substrates), V_G is the gate voltage, and V_{th} is the threshold voltage.

Theoretical Calculations. DFT calculations were performed with the Gaussian 16 program package without symmetry treatment.[s3] Initial structures were taken from X-ray crystal structure (cif files). The geometries were fully optimized using Becke's three parameter hybrid functional combined with the Lee-Yang-Parr correlation functional, denoted as the B3LYP level of density functional theory, with the 6-31G(d,p) basis set.[s4] Ground-state geometries were verified by the frequency calculations, where no imaginary frequency was found. Time-dependent DFT (TD-DFT) calculations was performed at 6-31G(d,p) level with a polarizable continuum (PCM) solvation model in chloroform.[s5] The nucleus-independent chemical shift (NICS(1)),[s6] 2D isochemical shielding surface ($ICSS_{zz}$)[s7] and anisotropy of the induced current density (ACID)[s8] calculation were performed at the 6-311G(d,p) level. Transfer integrals were calculated by ADF software[s9] using PBEO functional at the basis set of TZP.

Photothermal conversion efficiency. The photothermal conversion efficiency of **1** was determined according to the literature.[s10] To measure the photothermal conversion efficiency, a solution of NIR dyes in toluene was irradiated by a 940 nm laser at 3.5 W cm^2 for 10 min, and then the solution was cooled down to room temperature. The temperature of the solution was recorded at an interval of 10 s during this process. Detailed calculation was given as following:

$$\eta = hS\,\Delta T_{max} - Q_s/I\,(1 - 10^{-A)}) \quad (1)$$

where h is the heat transfer coefficient, S is the surface area of the container, and the value of hS is obtained from Eq. (1). The maximum steady temperature (T_{max}) of the solution and environmental temperature (T_{Surr}) were used. Qs expresses heat dissipated from the light absorbed by the solvent and a quartz cell. To gain hS, a dimensionless parameter is introduced as follows:

$\tau_s = m_D c_D / hS$ (2)

where m_D and c_D index the solution mass and heat capacity of toluene used as a solvent. A sample system time constant, τ_s, can be calculated; $t = -\tau_s \, ln(T - T_{Surr}/T_{Max} - T_{Surr})$ (3)

According to the obtained data and equations, the photothermal conversion efficiency of **1** was determined.

2. Synthesis

Table S1. Optimization of the reaction condition for synthesizing **1** and **2**. The reaction was conducted under an aerobic atmosphere.

Entries	Solvents	Metal salts	Time	Yield of 1	Yield of 2	Note
1	Pyridine	$Cu(OAc)_2$ (5.0 eq.)	3 h	28%	3%	
2	Pyridine	$FeCl_3$ (5.0 eq.)	2 h	-	-	No product formed
3	Pyridine	DDQ (60 eq.)	3 h	-	-	No product formed
4	Pyridine	TEMPO (60 eq.)	3 h	-	-	No reaction
5	Pyridine	AgOAc (10 eq.)	1 h	trace	-	Trace product
6	Pyridine	CuI (60 eq.)	60 h	19%	2%	
7	Pyridine	-	24 h	-	-	No reaction
8	Et_3N	$Cu(OAc)_2$ (5.0 eq.)	3 h	trace	-	Mainly recovery of **3**
9	Acetone	$Cu(OAc)_2$ (5.0 eq.)	3 h	-	-	No reaction
10	THF	$Cu(OAc)_2$ (5.0 eq.)	3 h	-	-	No reaction
11	MeOH	$Cu(OAc)_2$ (5.0 eq.)	3 h	-	-	No reaction
12	$CHCl_3$	$Cu(OAc)_2$ (5.0 eq.)	3 h	-	-	No reaction

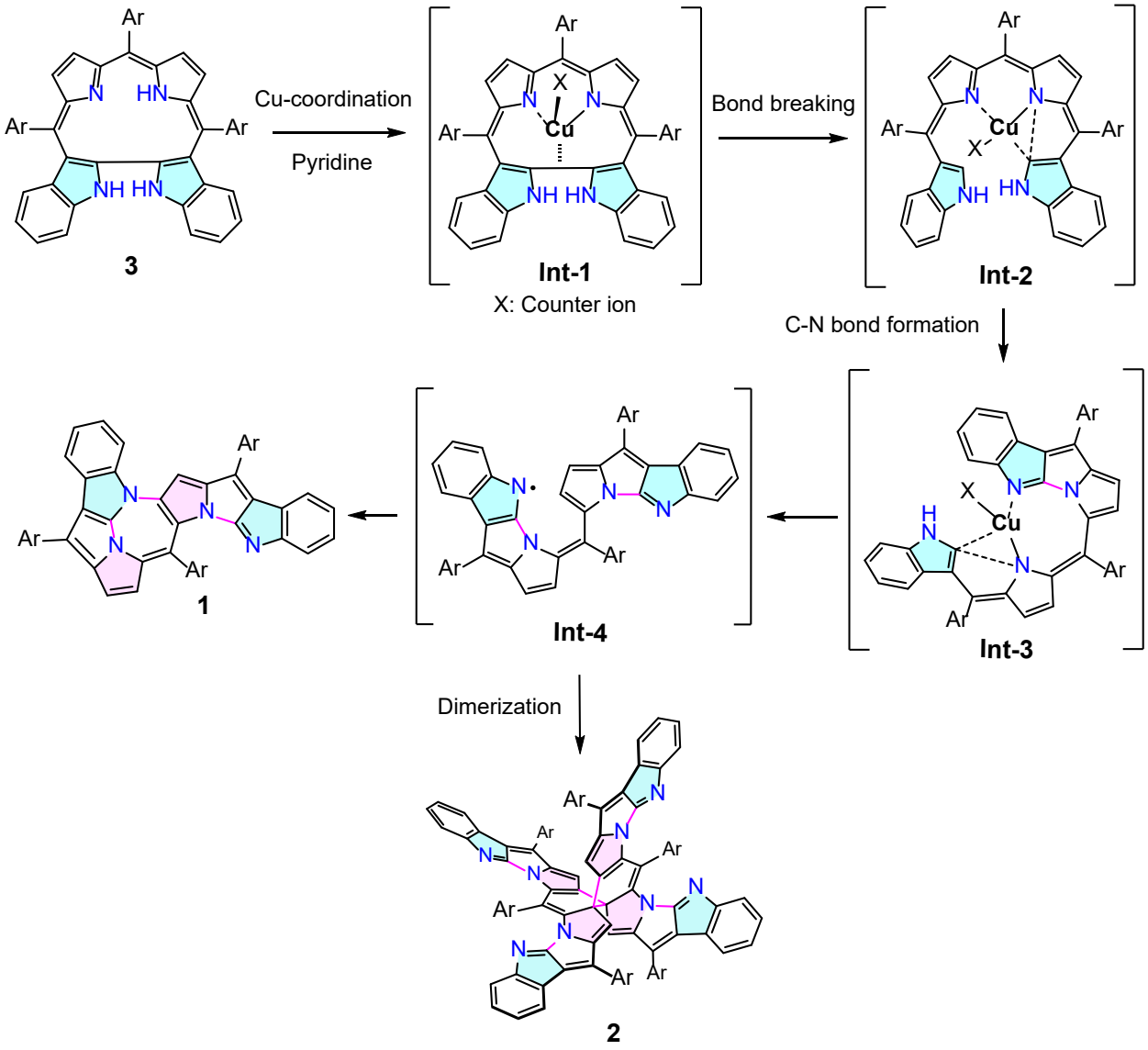

Scheme S1. Possible reaction routes for the formation of fused molecules **1** and **2** from the corrorin derivative **3**.

3. NMR Spectra

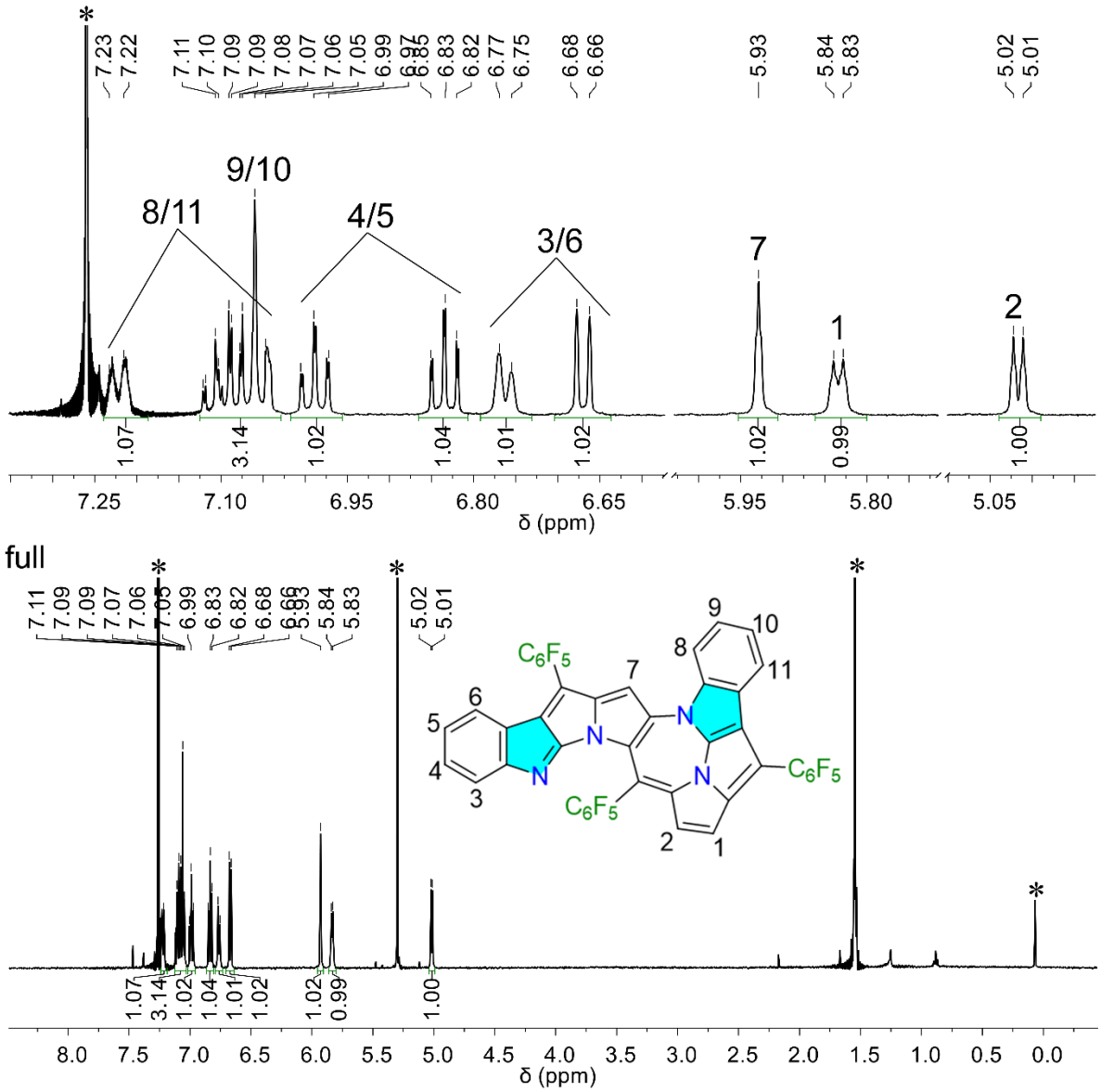

Fig. S1 ^{1}H-NMR spectrum of **1** determined in $CDCl_3$. Asterisks (*) represent solvent residue. Inset shows the corresponding labels for each proton of **1**.

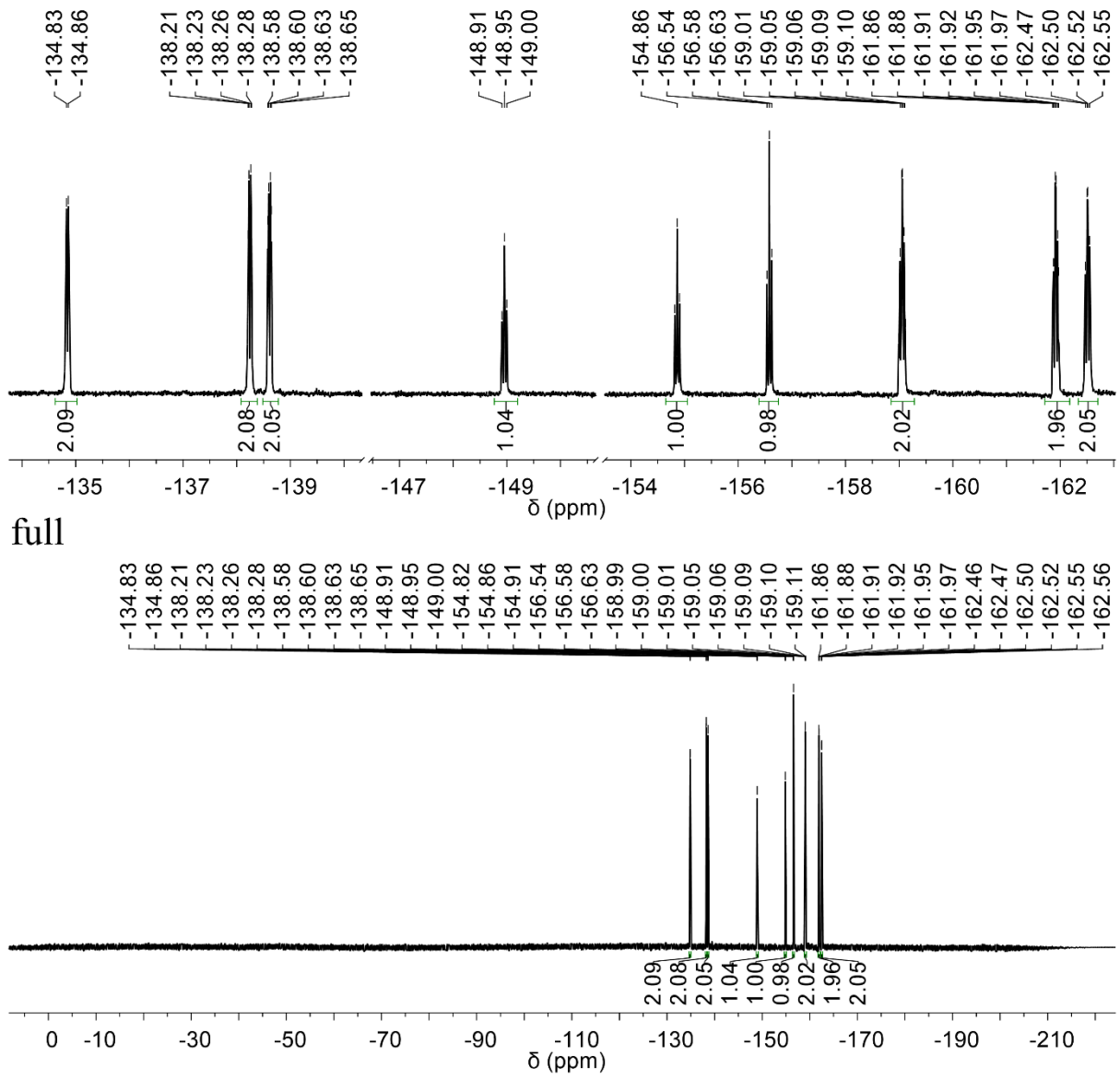

Fig. S2 ^{19}F-NMR spectrum of **1** determined in $CDCl_3$.

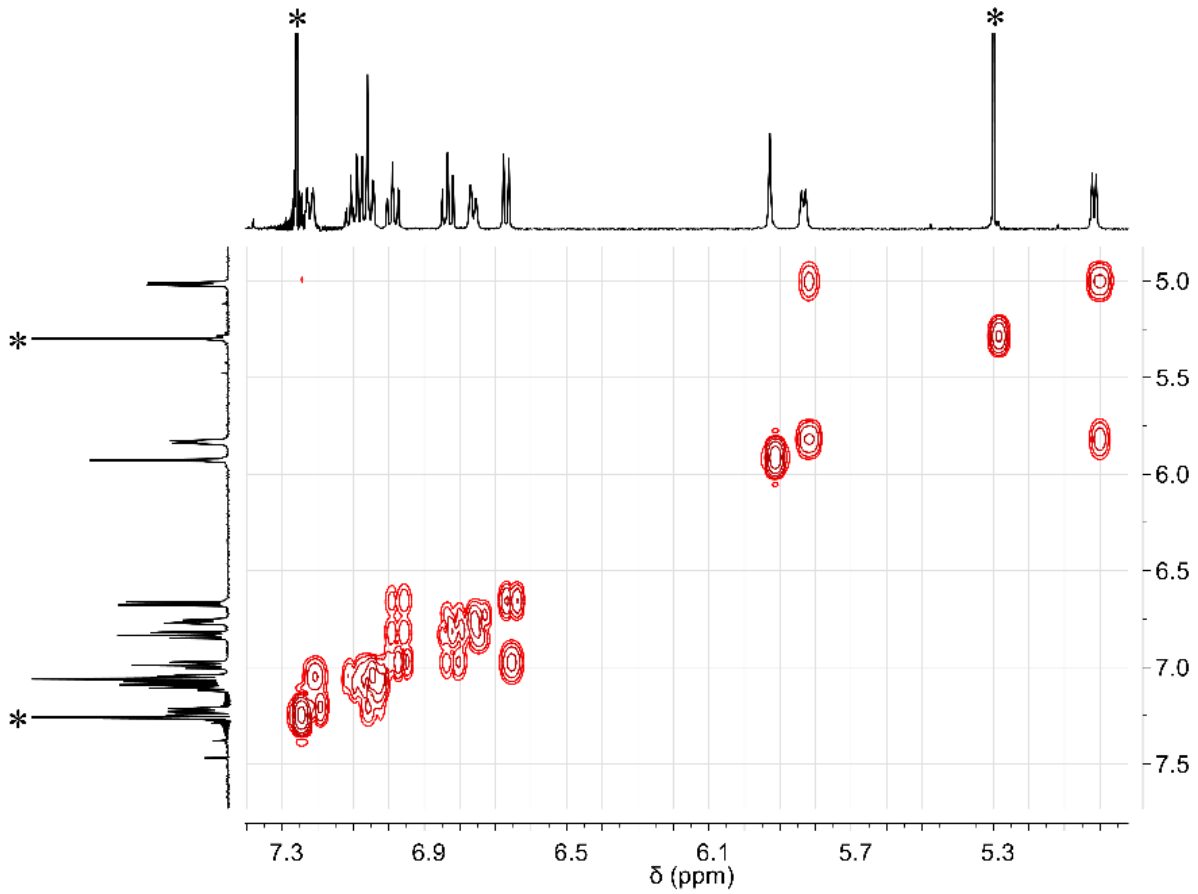

Fig. S3 ^{1}H-^{1}H COSY spectrum of compound **1** in $CDCl_3$. Asterisks (*) represent solvent residue.

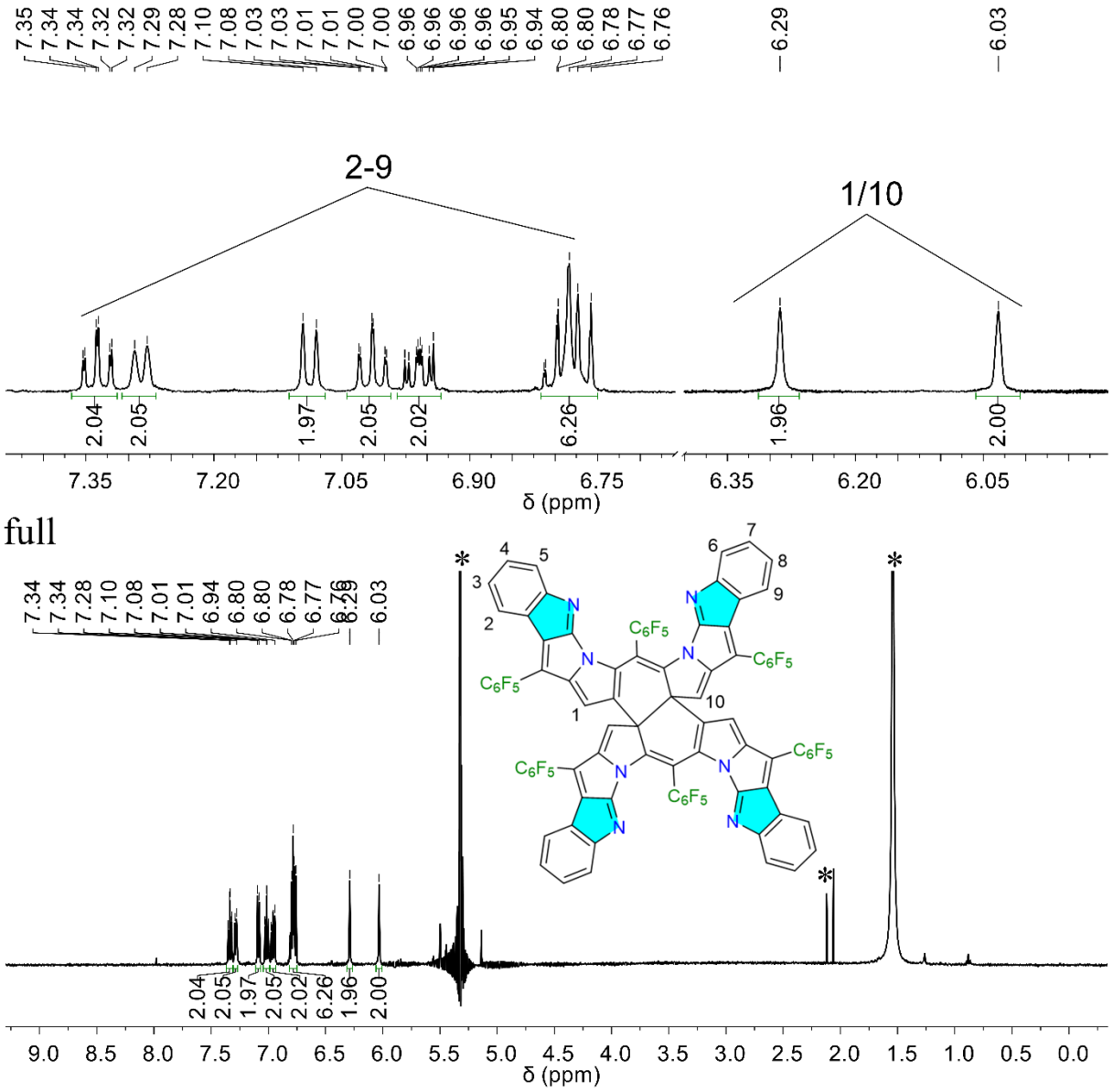

Fig. S4 ^{1}H-NMR spectrum of **2** determined in CD_2Cl_2. Inset shows the corresponding labels for each proton of **2**.

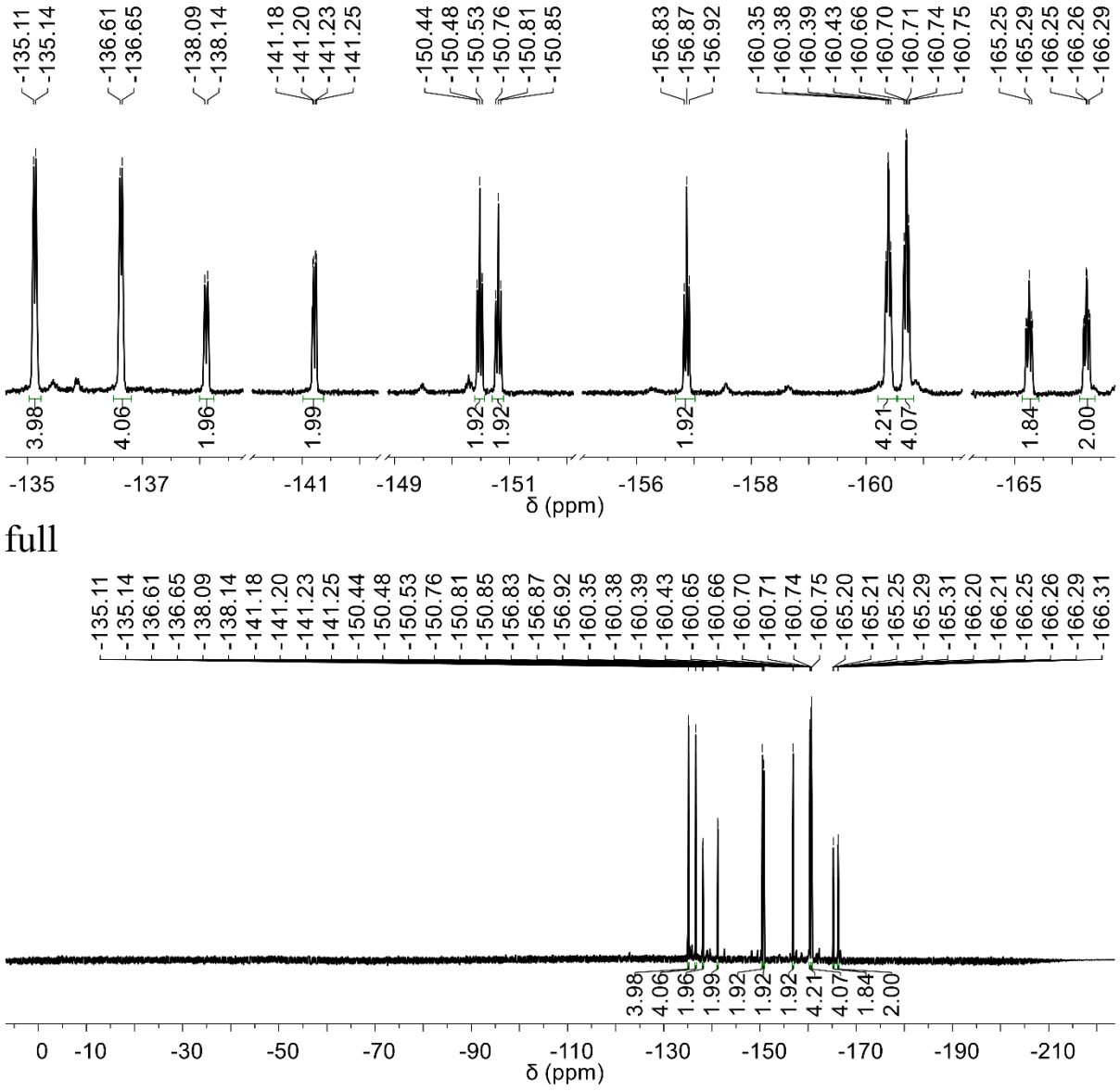

Fig. S5 ^{19}F-NMR spectrum of **2** determined in CD_2Cl_2.

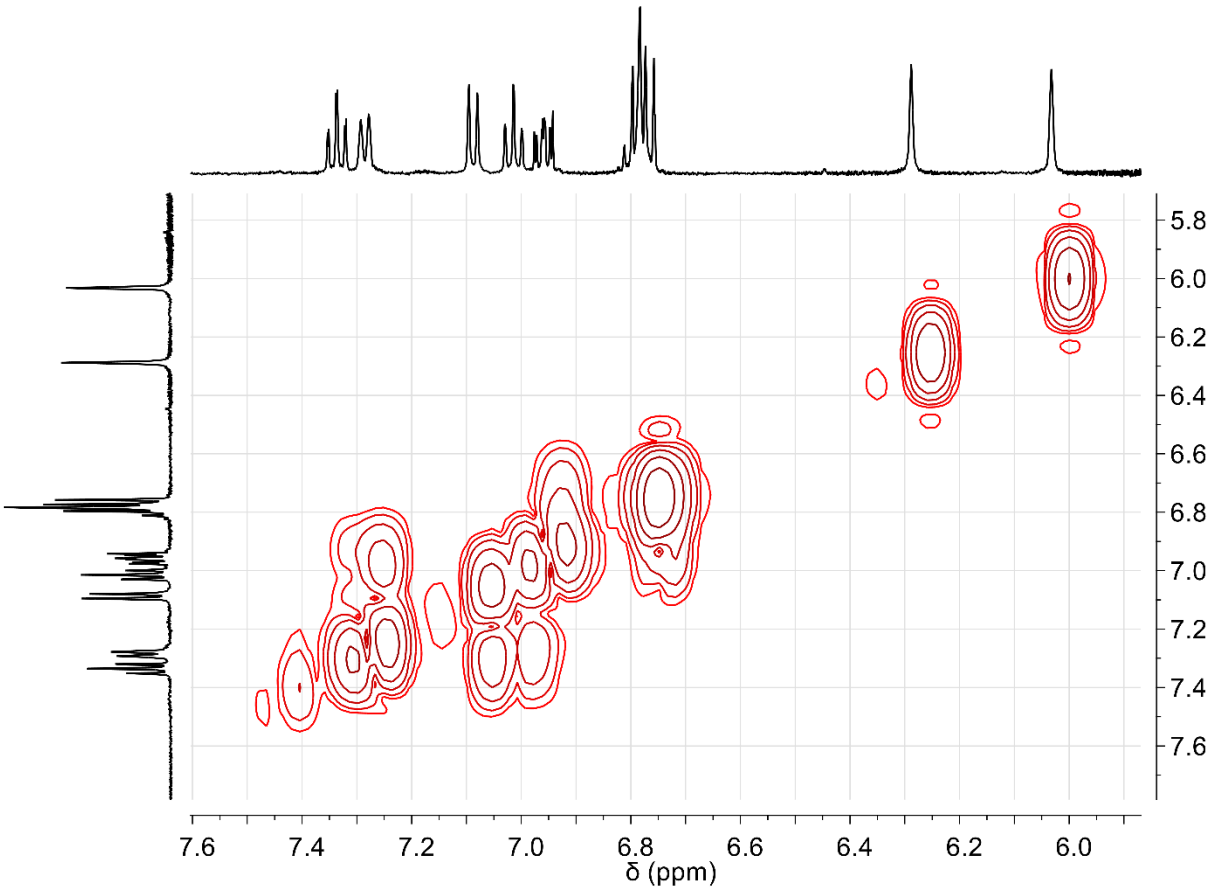

Fig. S6 ^{1}H-^{1}H COSY spectrum of **2** determined in CD_2Cl_2.

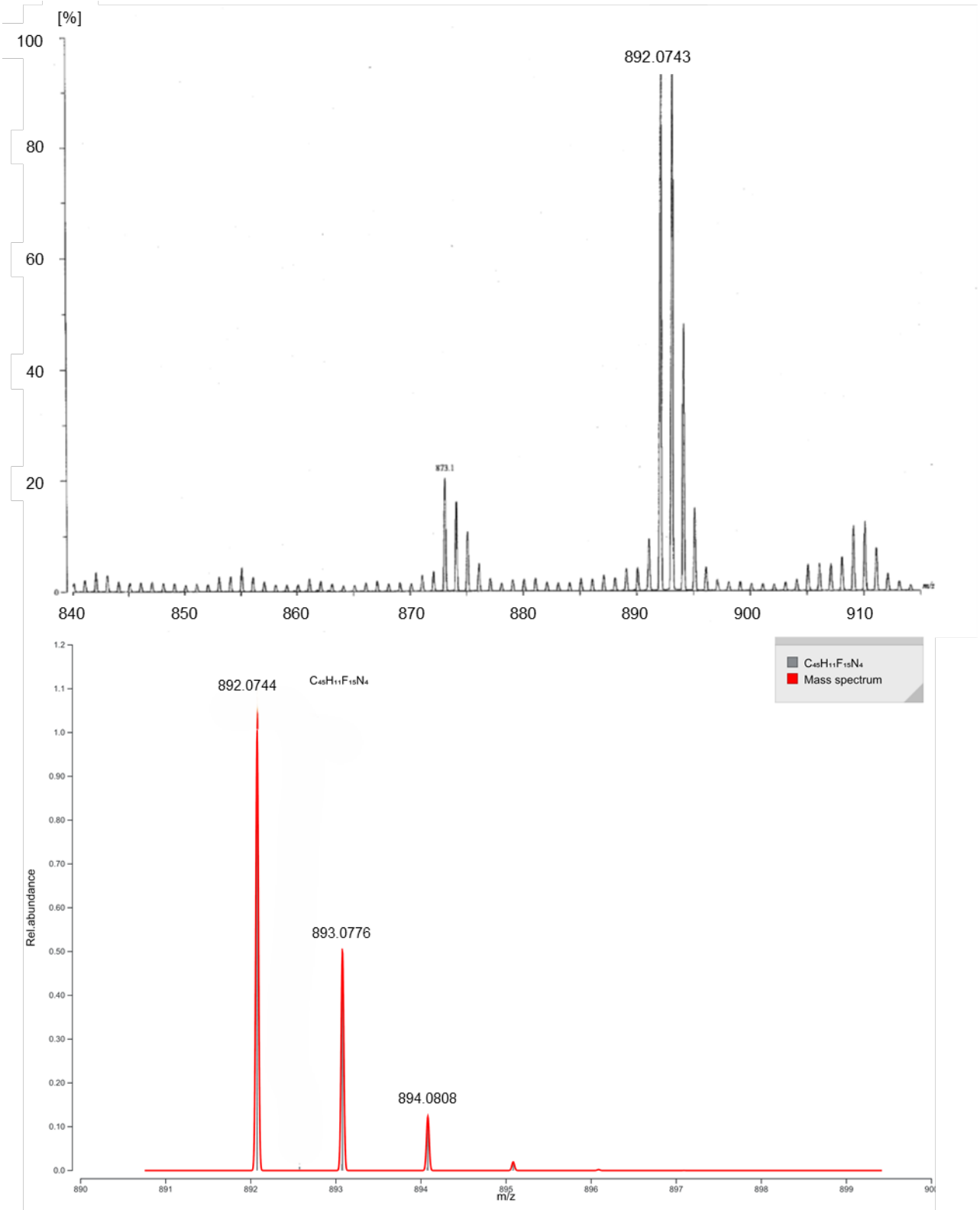

Fig. S7 FAB-HRMS of **1**.

[Molecular Formula]
Data : 18-fused-FAB(+)HR-2 Date : 18-Oct-2021 14:07
RT : 2.72 min Molecular Formula : C90 H20 F30 N8
Elements : C 90/90, H 21/20, F 30/30, N 8/8
Mass Tolerance : 1000ppm, 10mmu if m/z < 10, 1000mmu if m/z > 1000
Unsaturation (U.S.) : -0.5 - 90.0

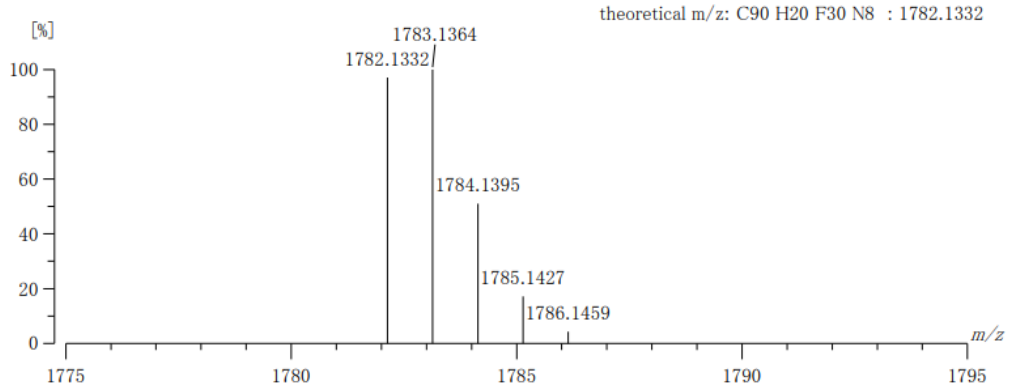

[Mass Spectrum]
Data : 18-fused-FAB(+)HR-2 Date : 18-Oct-2021 14:07
Instrument : MStation JMS-700
Note : IMCE Kyushu Univ.
Ion Mode : FAB+
Scan# : 34
Cut Level : 1.00 %
Matrix:3NBA (136,154,289,307,460,613)
External standard:PEG

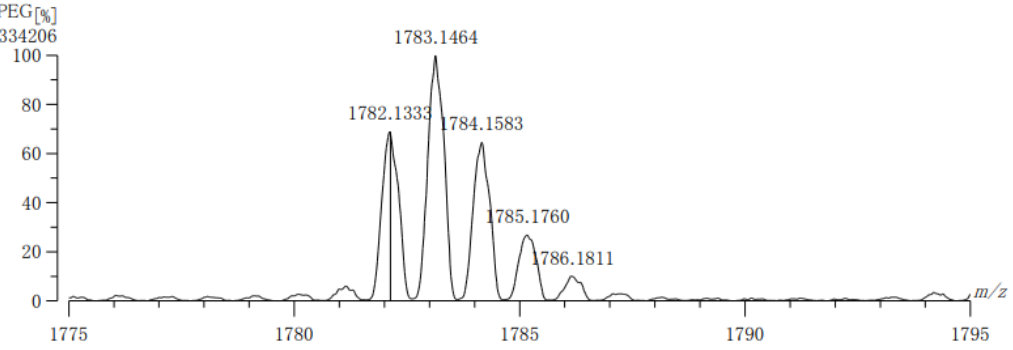

	Observed m/z	Int%	Err[ppm / mmu]	U.S.	Composition
1	1782.1333	68.83	+0.1 / +0.1	70.0	C90 H20 F30 N8

Fig. S8 FAB-HRMS of **2**.

4. Single Crystal X-ray Crystallography

Table S2. Summary of X-ray crystallographic data for **1** and **2**.

compound	**1**	**2**
formula	$C_{46}H_{12}Cl_3F_{15}N_4$	$C_{106.64}H_{57.83}F_{30}N_8$
formula weight	1011.95	2021.12
habit	needle	block
***T*(K)**	100	100
crystal system	triclinic	triclinic
space group	*P* -1	*P* -1
***a* (Å)**	9.6719(5)	13.2666(4)
***b* (Å)**	14.2671(8)	19.1346(5)
***c* (Å)**	15.0220(7)	21.0002(6)
α (deg.)	111.646(5)	84.990(2)
β (deg.)	90.926(4)	76.702(3)
γ (deg.)	97.372(4)	84.645(2)
***V* (Å^3)**	1906.24(18)	5153.4(3)
Z	2	2
ρ_{calc}(g/cm^3)	1.763	1.302
***F*$_{000}$**	1004.0	2047.0
crystal size(mm^3)	0.2x0.05x0.02	0.1x0.1x0.01
2θ_{max}(deg.)	56	56
***R*$_1$(*I* > 2σ(*I*))**	0.0752	0.0854
***wR*$_2$(all data)**	0.2129	0.2498
GOF	1.052	0.989

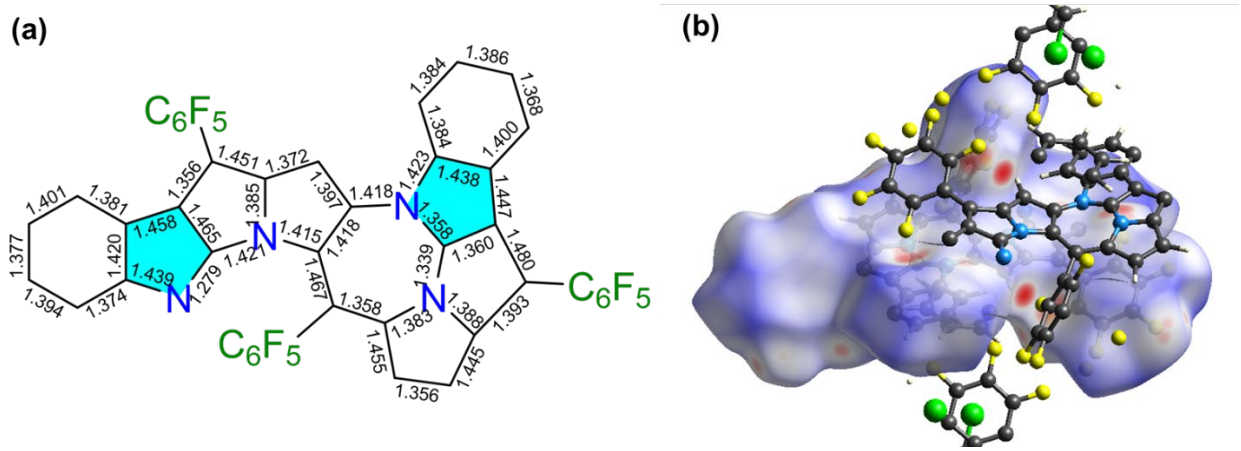

Fig. S9 (a) Selected bond lengths (Å) of **1** and (b) Hirshfeld surface analysis plot showing intermolecular interactions over compound **1**.

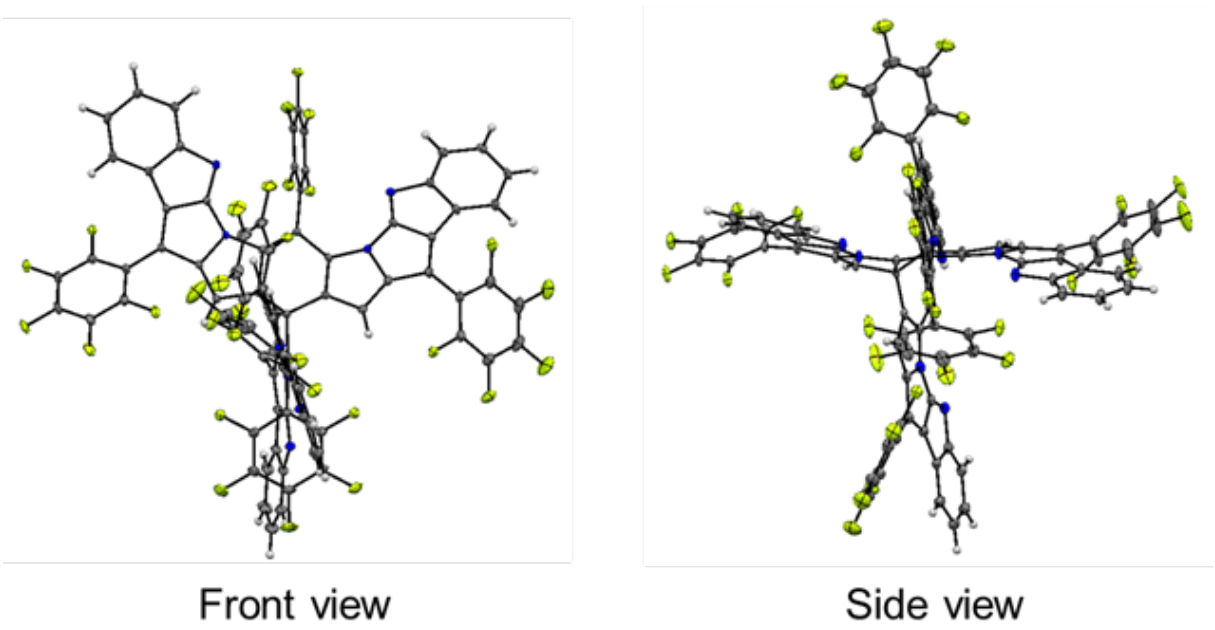

Fig. S10 Front and side views of X-ray crystal structures of **2** with thermal ellipsoids of 50% probability.

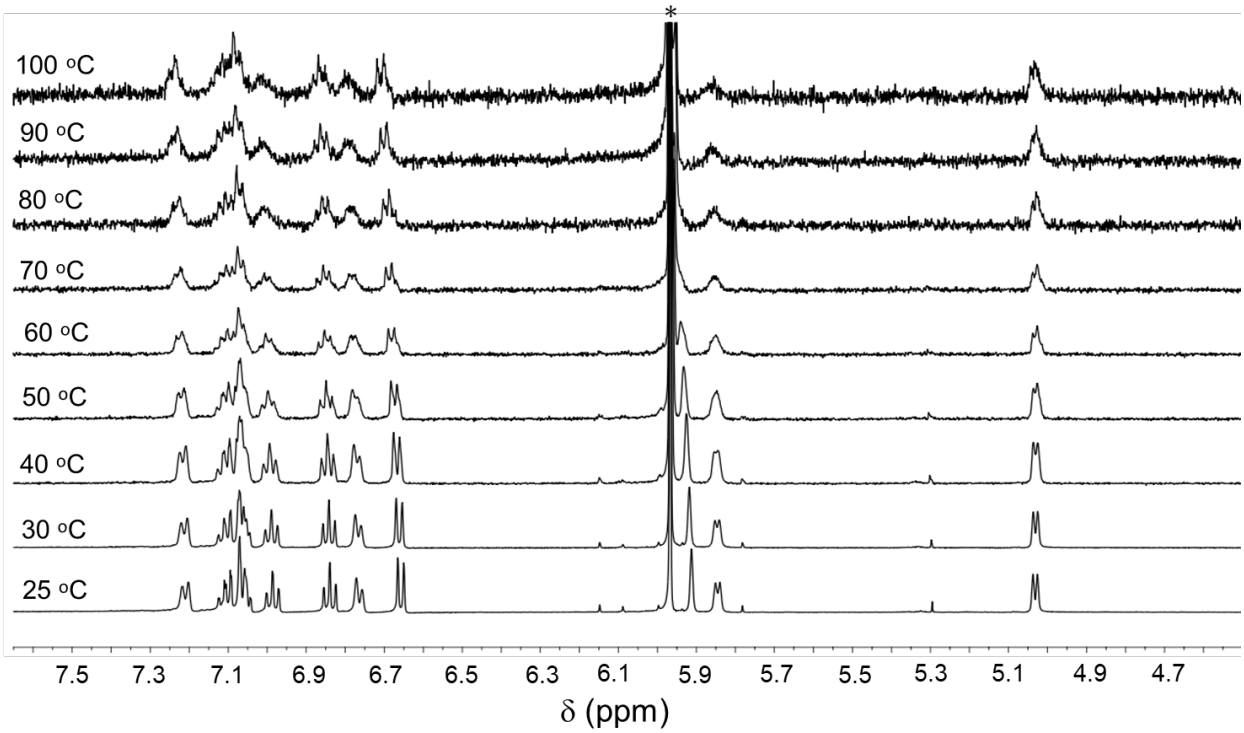

Fig. S11 Variable temperature ^{1}H-NMR spectra of **1** recorded in $C_2D_4Cl_4$. Asterisks (*) represent solvent residue.

5. Spectroscopies

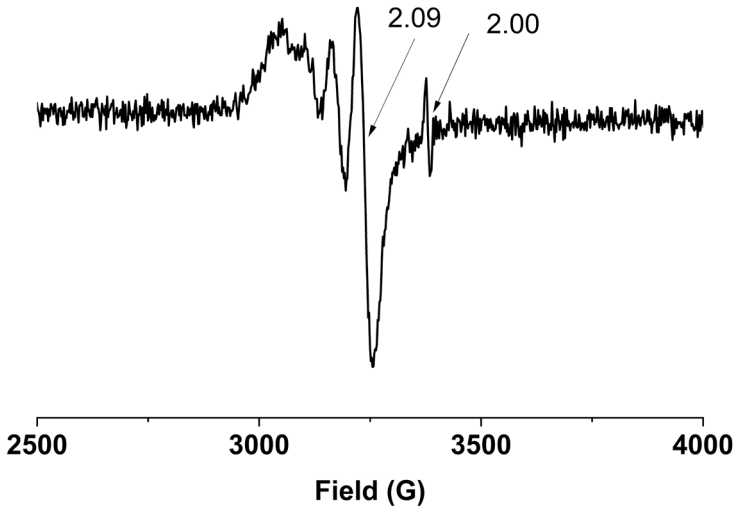

Fig. S12 EPR spectrum of the reaction mixture of **3** in the presence of $Cu(OAc)_2$ in pyridine at 298 K.

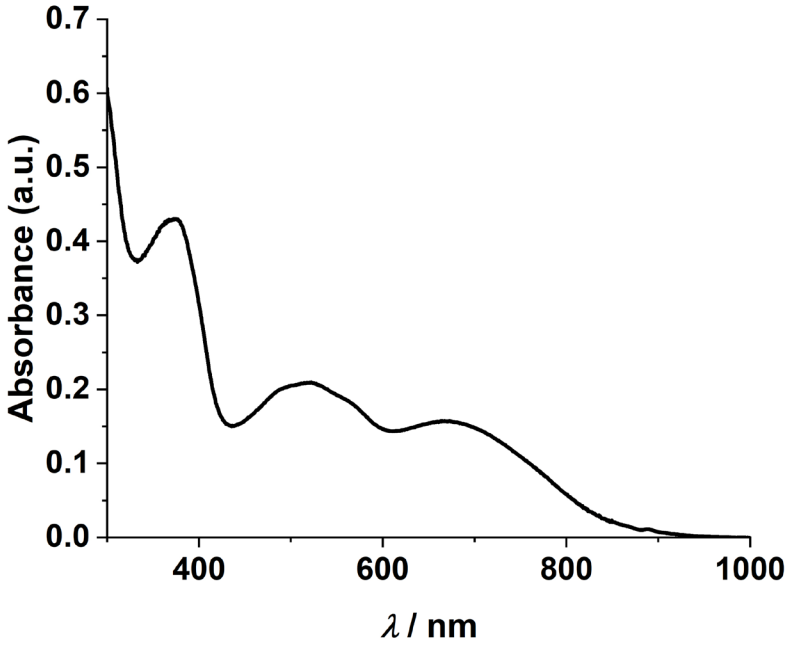

Fig. S13 UV/vis/NIR absorption spectrum of **2** in CH_2Cl_2.

6. Density-Functional Theory (DFT) Calculations

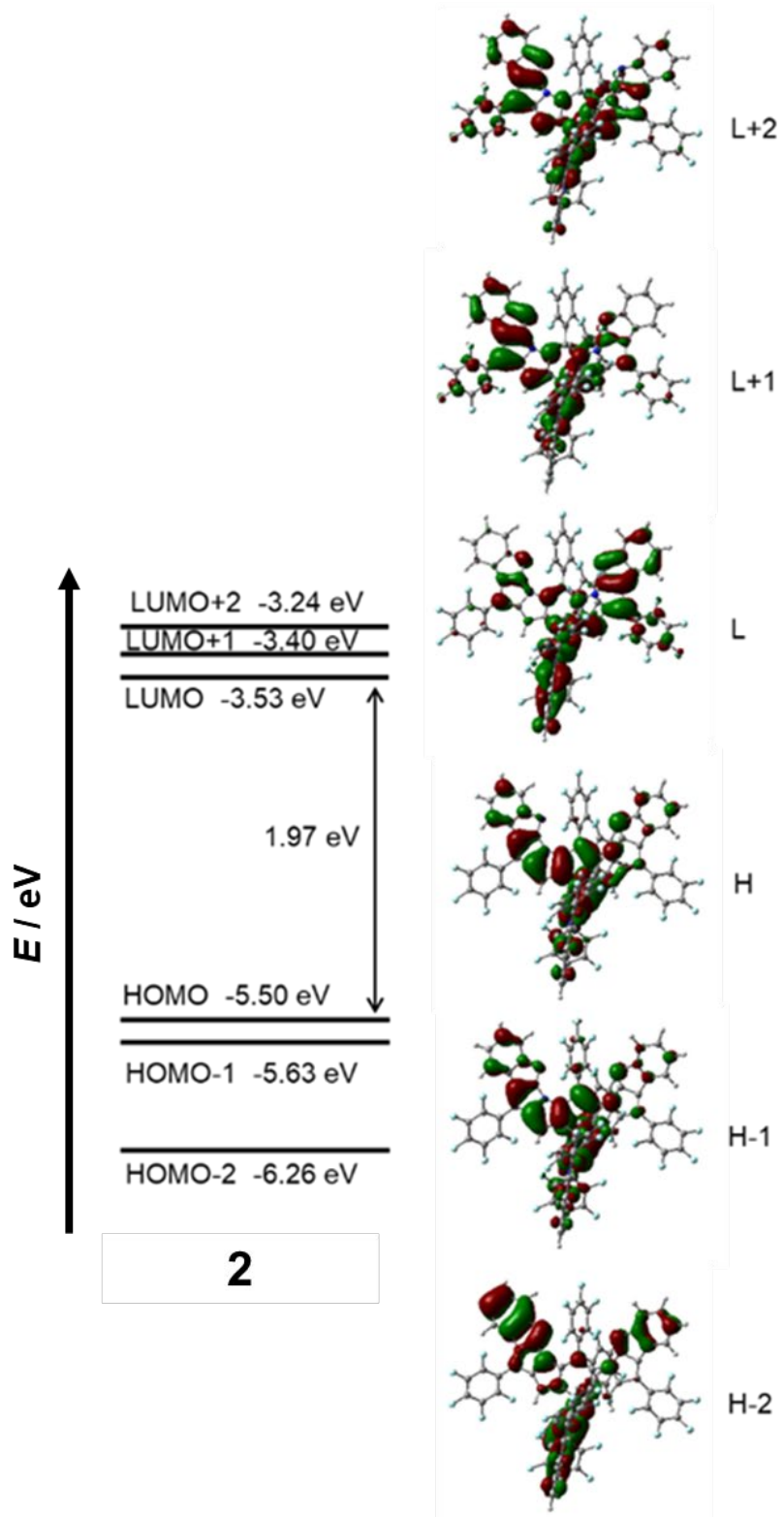

Fig. S14 Molecular orbital diagram of **2** at the B3LYP/6-31G(d,p) level of theory.

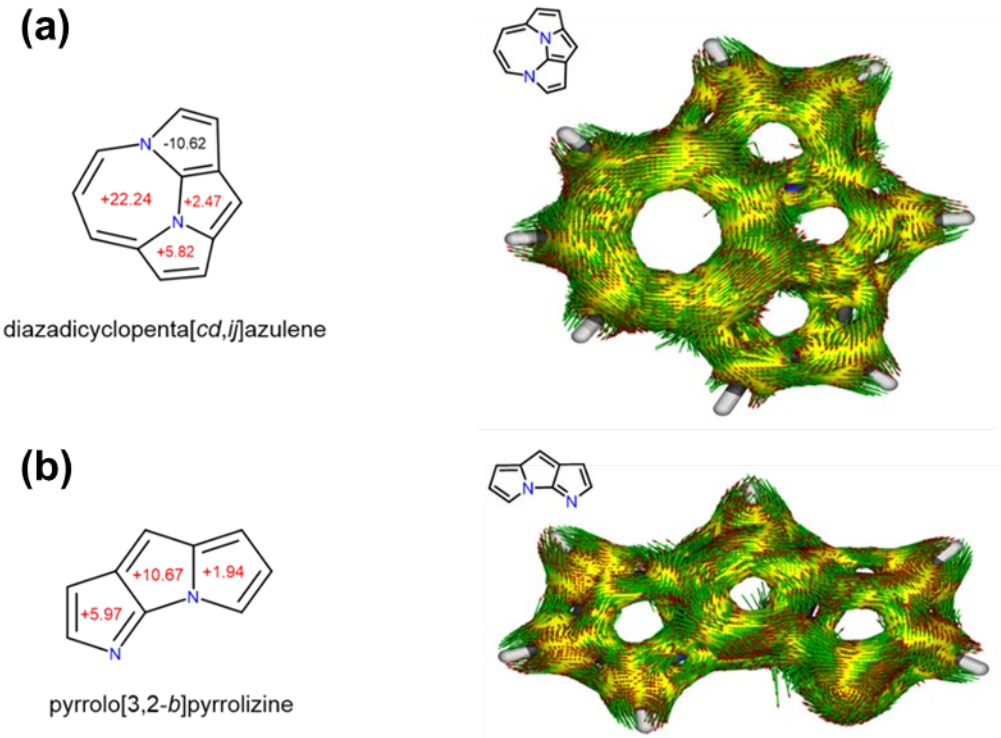

Fig. S15 NICS(1) values (left) and ACID plot (right) of (a) diazadicyclopenta[*cd,ij*]azulene and (b) pyrrolo[3,2-*b*]pyrrolizine obtained by B3LYP/6-311G(d,p) level. Isovalue is set to 0.05.

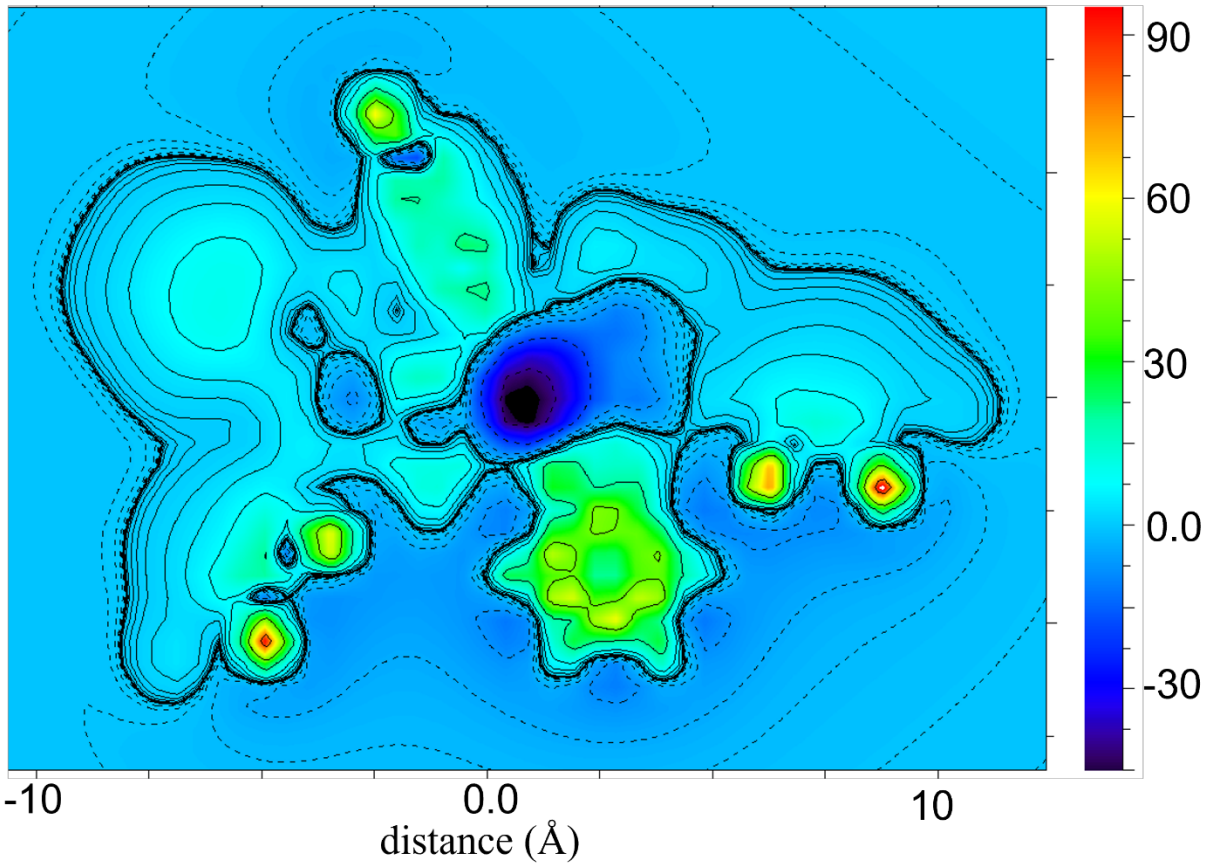

Fig. S16 2D ICSS$(1)_{zz}$ map of **1** probed at 1 Å above the XY plane at the B3LYP/6-311G(d,p) level of theory (employed for both geometry optimization and ICSS calculation).

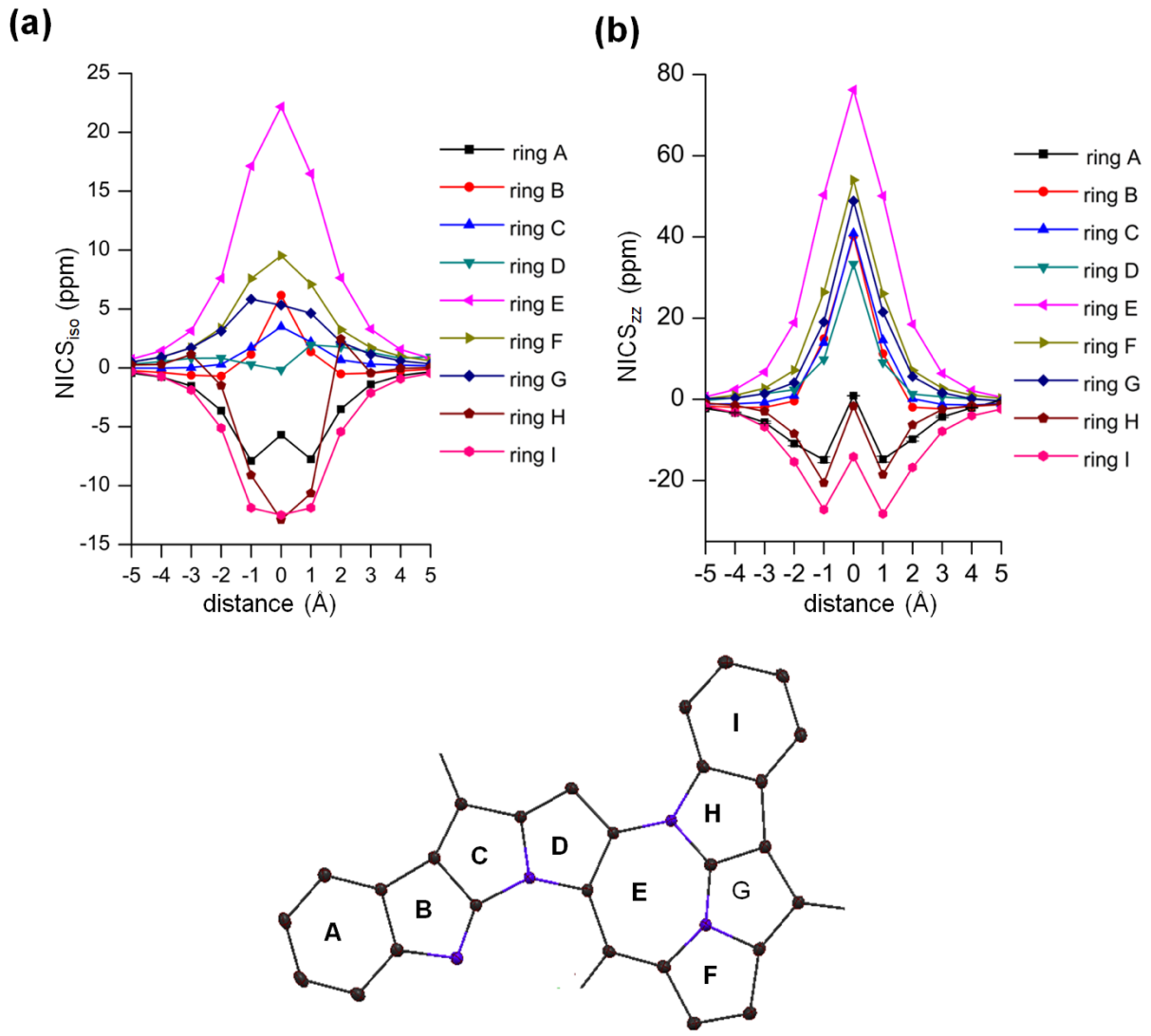

Fig. S17 Plot of (a) NICS$_{iso}$ and (b) NICS$_{zz}$ in ppm vs distance in Å from the plane of the ring A to I of compound **1** at the B3LYP/6-311G(d,p) level of theory.

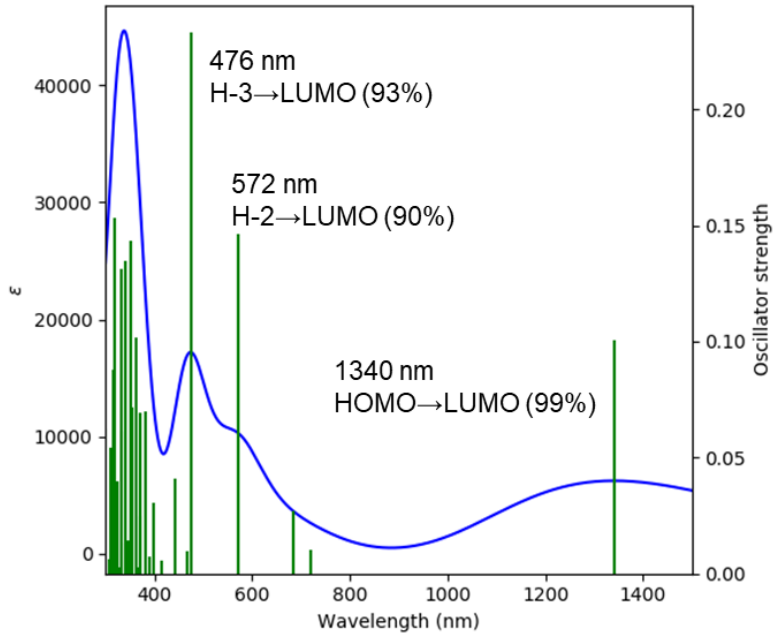

Fig. S18 Simulated absorption spectrum of **1** along with the calculated transitions (green) obtained by TD-DFT (B3LYP) method. The specific compositions of the transitions are given in inset.

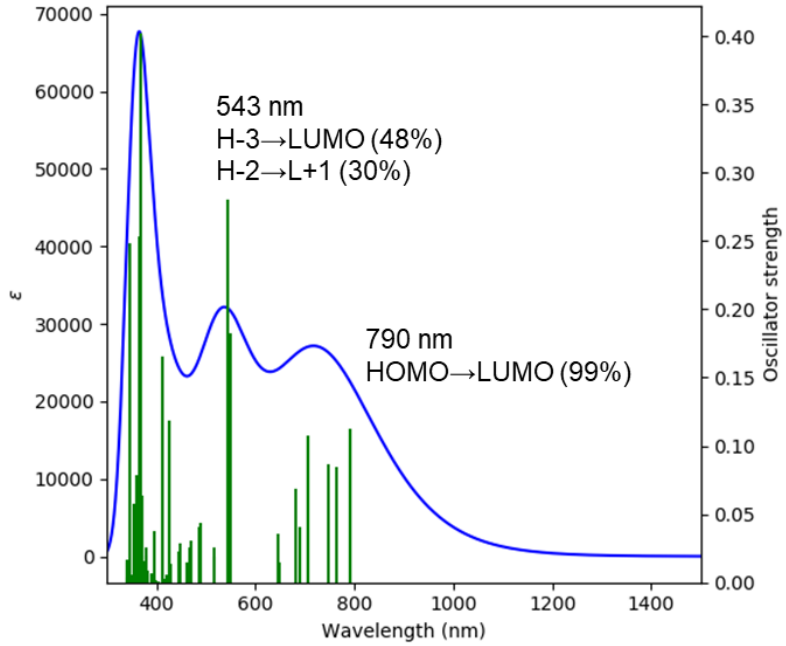

Fig. S19 Simulated absorption spectrum of **2** along with the calculated transitions (green) obtained by TD-DFT (B3LYP) method. The specific compositions of the transitions are given in inset.

7. Cartesian Coordinates

Table S3. Cartesian coordinates of the DFT optimized geometry for **1**.

Symbol	X	Y	Z
F	6.16739	-1.79575	1.38944
F	8.82686	-1.99068	1.127
F	10.1306	-0.58128	-0.81281
F	8.70991	1.01335	-2.50901
F	6.0478	1.19317	-2.29872
F	-3.44386	-3.16827	1.66969
F	-4.88433	-5.4253	1.5124
F	-6.7064	-5.76022	-0.48387
F	-7.06121	-3.80053	-2.34333
F	-5.61121	-1.54632	-2.22705
F	-0.85797	2.02649	2.75509
F	-2.15775	4.27284	3.49869
F	-2.39222	6.35486	1.75573
F	-1.31377	6.17444	-0.73577
F	-0.03326	3.93324	-1.50023
N	2.41936	0.61381	-0.37656
N	1.30085	-1.4297	0.43915
N	-3.14835	2.40993	-0.36825
N	-1.82112	0.34192	0.08667
C	1.64143	1.74665	-0.11279
C	2.57744	2.85394	-0.26536
H	2.30381	3.89439	-0.21117
C	3.81985	2.36157	-0.55251
H	4.70572	2.95058	-0.73236
C	3.76815	0.91815	-0.56416
C	4.53134	-0.23763	-0.34735
C	3.57712	-1.28231	0.042
C	2.35	-0.66677	0.04001
C	3.28053	-2.64205	0.46148
C	4.03662	-3.80044	0.6642
H	5.1024	-3.79233	0.48147
C	3.41698	-4.95681	1.12322
H	4.00755	-5.85199	1.27915
C	2.04635	-4.97726	1.40459
H	1.58841	-5.88273	1.785
C	1.25629	-3.84754	1.21176
H	0.20565	-3.86944	1.46652
C	1.86485	-2.69615	0.7209
C	-0.02727	-0.96237	0.30714

C	-1.16349	-1.79586	0.20684
H	-1.16855	-2.87069	0.21509
C	-2.2594	-0.97137	0.07972
C	-3.69149	-1.02329	-0.2009
C	-4.09288	0.27156	-0.40023
C	-5.17398	1.1997	-0.6783
C	-6.53607	1.10161	-0.93072
H	-7.0339	0.1414	-0.96482
C	-7.26499	2.27735	-1.15551
H	-8.3284	2.21306	-1.3539
C	-6.64337	3.52268	-1.1313
H	-7.22828	4.41731	-1.31042
C	-5.2676	3.6383	-0.87877
H	-4.77528	4.60296	-0.85813
C	-4.54794	2.48186	-0.65444
C	-2.93125	1.15189	-0.22957
C	-0.42189	0.39381	0.22223
C	0.31586	1.66322	0.21834
C	5.98482	-0.31698	-0.45854
C	6.75823	-1.11161	0.39937
C	8.13673	-1.21686	0.28357
C	8.8042	-0.49684	-0.69915
C	8.07724	0.31822	-1.5585
C	6.69834	0.39957	-1.43272
C	-4.47407	-2.26197	-0.27107
C	-4.31703	-3.29615	0.66138
C	-5.0567	-4.4683	0.59839
C	-5.99048	-4.64026	-0.41703
C	-6.17249	-3.63732	-1.3613
C	-5.41896	-2.47421	-1.28308
C	-0.38255	2.9134	0.61162
C	-0.95089	3.03925	1.88039
C	-1.62591	4.18436	2.27565
C	-1.73962	5.24925	1.3912
C	-1.17879	5.15897	0.12461
C	-0.51652	4.00093	-0.25179

Table S4. Cartesian coordinates of the DFT optimized geometry for **2**.

Symbol	X	Y	Z
F	-3.44367	-3.16832	1.669543
F	-4.8841	-5.42538	1.512289
F	-6.70662	-5.76009	-0.48362
F	-7.0617	-3.80031	-2.34291
F	-5.6117	-1.54609	-2.22672
F	-0.85769	2.026797	2.754897
F	-2.15717	4.273364	3.498368
F	-2.39148	6.355267	1.75526
F	-1.31321	6.174491	-0.73631
F	-0.03311	3.933081	-1.5007
F	6.167088	-1.79609	1.389399
F	8.826636	-1.99097	1.127454
F	10.13072	-0.58129	-0.8119
F	8.71036	1.013448	-2.50825
F	6.048184	1.193147	-2.29852
N	-1.82124	0.341973	0.086811
N	-3.14856	2.410027	-0.36772
N	2.419434	0.613694	-0.37687
N	1.300726	-1.42991	0.438257
C	-0.42195	0.393783	0.222048
C	-0.02739	-0.96243	0.306699
C	-1.16364	-1.79586	0.206496
H	-1.16865	-2.87069	0.214534
C	-2.25955	-0.97133	0.079742
C	-3.69163	-1.02321	-0.2009
C	-4.09299	0.271638	-0.4002
C	-2.93138	1.151962	-0.22942
C	-5.17416	1.199807	-0.67796
C	-6.53627	1.101711	-0.93022
H	-7.03404	0.141482	-0.96449
C	-7.26526	2.27748	-1.15466
H	-8.32868	2.213195	-1.35298
C	-6.64369	3.522819	-1.13019
H	-7.22866	4.417465	-1.30904
C	-5.26789	3.638443	-0.87778
H	-4.77565	4.60314	-0.85688
C	-4.54816	2.481974	-0.65384
C	0.315909	1.663141	0.21807
C	1.641466	1.746506	-0.11312
C	2.577536	2.853794	-0.26544
H	2.30395	3.894246	-0.21113

C	3.820005	2.361446	-0.55231
H	4.705927	2.950463	-0.73186
C	3.768267	0.918033	-0.56413
C	4.53136	-0.23784	-0.34757
C	3.577001	-1.28266	0.041167
C	2.349889	-0.66707	0.03902
C	3.280355	-2.6423	0.4609
C	4.036355	-3.80072	0.663798
H	5.10213	-3.79275	0.481053
C	3.416629	-4.95698	1.122966
H	4.007157	-5.85217	1.279036
C	2.045986	-4.97735	1.404257
H	1.588008	-5.88276	1.784768
C	1.255991	-3.84764	1.211187
H	0.205316	-3.86941	1.465804
C	1.864651	-2.69632	0.720275
C	-4.47418	-2.2619	-0.27101
C	-4.31701	-3.29614	0.661353
C	-5.05665	-4.4683	0.598389
C	-5.99065	-4.64017	-0.41684
C	-6.17279	-3.63718	-1.36103
C	-5.41927	-2.47407	-1.28285
C	-0.38241	2.913395	0.611257
C	-0.95062	3.039474	1.880077
C	-1.62544	4.184691	2.275286
C	-1.73906	5.249524	1.39076
C	-1.17839	5.159048	0.124139
C	-0.5163	4.000877	-0.25222
C	5.984865	-0.3172	-0.45852
C	6.758122	-1.11189	0.399482
C	8.136633	-1.2171	0.283962
C	8.804288	-0.49692	-0.69852
C	8.077495	0.31818	-1.55795
C	6.69856	0.399472	-1.43246

8. References

(s1) B. Basumatary, I. Hashiguchi, S. Mori, S. Shimizu, M. Ishida and H. Furuta, *Angew. Chem. Int. Ed.,* 2020, **59**, 15897.

(s2) (*a*) SIR2004: M. C. Burla, R. Caliandro, M. Camalli, B. Carrozzini, G. L. Cascarano, L. De Caro, C. Giacovazzo, G. Polidori and R. Spagna, *J. Appl. Cryst.,* 2005, **38**, 381; (*b*) SIR2011: M. C. Burla, R. Caliandro, M. Camalli, B. Carrozzini, G. L. Cascarano, L. De Caro, C. Giacovazzo, G. Polidori and R. Spagna*, J. Appl. Cryst.,* 2012, **45**, 357; (*c*) SHELXT Version 2014/5: G. M. Sheldrick, *Acta Cryst.,* 2015, **A71**, 3; (*d*) SHELXL-2013, 2014/7: G. M. Sheldrick, *Acta Cryst.,* 2015, **C71**, 3.

(s3) Gaussian 16, Revision A.03, M. J. Frisch, G. W. Trucks, H. B. Schlegel, G. E. Scuseria, M. A. Robb, J. R. Cheeseman, G. Scalmani, V. Barone, G. A. Petersson, H. Nakatsuji, X. Li, M. Caricato, A. V. Marenich, J. Bloino, B. G. Janesko, R. Gomperts, B. Mennucci, H. P. Hratchian, J. V. Ortiz, A. F. Izmaylov, J. L. Sonnenberg, D. Williams-Young, F. Ding, F. Lipparini, F. Egidi, J. Goings, B. Peng, A. Petrone, T. Henderson, D. Ranasinghe, V. G. Zakrzewski, J. Gao, N. Rega, G. Zheng, W. Liang, M. Hada, M. Ehara, K. Toyota, R. Fukuda, J. Hasegawa, M. Ishida, T. Nakajima, Y. Honda, O. Kitao, H. Nakai, T. Vreven, K. Throssell, J. A. Montgomery, Jr., J. E. Peralta, F. Ogliaro, M. J. Bearpark, J. J. Heyd, E. N. Brothers, K. N. Kudin, V. N. Staroverov, T. A. Keith, R. Kobayashi, J. Normand, K. Raghavachari, A. P. Rendell, J. C. Burant, S. S. Iyengar, J. Tomasi, M. Cossi, J. M. Millam, M. Klene, C. Adamo, R. Cammi, J. W. Ochterski, R. L. Martin, K. Morokuma, O. Farkas, J. B. Foresman and D. J. Fox, Gaussian, Inc., Wallingford CT, 2016.

(s4) (*a*) F. Neese, Wiley Interdis. Rev.; *Comput. Mol. Sci*., 2012, **2**, 73; (*b*) Y. S. Lee, W. C. Ermler and K. S. Pitzer, *J. Chem. Phys*., 1977*,* **67**, 5861; (*c*) B. Metz, H. Stoll and M. Dolg, *J. Chem. Phys*., 2000, **113**, 2563.

(s5) (*a*) V. Barone and M. Cossi, *J. Phys. Chem. A,* 1998, **102**, 1995; (*b*) M. Cossi, N. Rega, G. Scalmani and V. Barone, *J. Comput. Chem*., 2003, **24**, 669.

(s6) Z. Chen, C. S. Wannere, C. Corminboeuf, R. Puchta and P. V. R. Schleyer, *Chem. Rev*., 2005, **105**, 3842.

(s7) (*a*) S. Klod and E. Kleinpeter, *J. Chem. Soc., Perkin Trans. 2*, 2001, 1893; (*b*) T. Lu and F. Chen, *J. Comput. Chem.,* 2012, **33**, 580.

(s8) R. Herges and D. Geuenich, *J. Phys. Chem. A*, 2001, **105**, 3214.

(s9) G. te Velde, F.M. Bickelhaupt, E.J. Baerends, C. Fonseca Guerra, S.J.A. van Gisbergen, J.G. Snijders and T. Ziegler, *J. Comput. Chem.,* 2001*,* **22**, 931.

(s10) Q. Tian, F. Jiang, R. Zou, Q. Liu, Z. Chen, M. Zhu, S. Yang, J. Wang, J. Wang and J. Hu, *ACS Nano*, 2011, **5**, 9761.